

## Reconstructions and nonstoichiometry of oxygenated $\beta$ -Si<sub>3</sub>N<sub>4</sub> (10 $\bar{1}$ 0) surfaces

Weronika Walkosz, Juan C. Idrobo,\* Robert F. Klie, and Serdar Ögüt

*Department of Physics, University of Illinois at Chicago, Chicago, Illinois 60607, USA*

(Received 27 August 2008; published 23 October 2008)

Motivated by the recent electron microscopy studies indicating the presence of oxygen at the silicon nitride/rare-earth oxide interfaces, results from an extensive set of first-principles calculations are presented for the preferred bonding sites and configurations of O on the  $\beta$ -Si<sub>3</sub>N<sub>4</sub> (10 $\bar{1}$ 0) surface as a function of coverage and surface stoichiometry. Most of the energetically favorable oxygenated  $\beta$ -Si<sub>3</sub>N<sub>4</sub> (10 $\bar{1}$ 0) surfaces are predicted to exhibit reconstructions and nonstoichiometry as O replaces N to achieve bridging configurations between two Si atoms. The structural stability of most of the low-energy structures is driven by tendency of the surface atoms to saturate their dangling bonds while preserving close-to-ideal coordination and bond angles. The implications of these first-principles results in light of the recent experimental studies and previous computational studies on the bare surface are discussed.

DOI: [10.1103/PhysRevB.78.165322](https://doi.org/10.1103/PhysRevB.78.165322)

PACS number(s): 68.43.Bc, 68.43.Fg, 68.35.bg

### I. INTRODUCTION

The growing interest in silicon nitride ceramics results from their desirable physical and mechanical properties in many high temperature and pressure applications.<sup>1</sup> Good resistance to oxidation, low coefficient of friction, negligible creep, and high decomposition temperatures are some of these important properties. The widespread use and reliability of Si<sub>3</sub>N<sub>4</sub> ceramics as structural components are, however, limited by their brittleness. Rare-earth oxides (REOs), when included as sintering additives in the microstructural design of Si<sub>3</sub>N<sub>4</sub> ceramics, have long been empirically known to overcome this problem by forming an intergranular film (IGF) surrounding the matrix grains of the ceramic.<sup>2</sup> The resulting microstructure has been shown to effectively control the evolution and mechanical properties of Si<sub>3</sub>N<sub>4</sub>, such as its toughness and strength. Scientific efforts aimed at achieving a more detailed atomic-scale understanding of how the different additives bond to the Si<sub>3</sub>N<sub>4</sub> grains and how they affect the mechanical properties of the material are, therefore, of both fundamental and technological interests. As examples of such efforts, the recent experimental studies at the Si<sub>3</sub>N<sub>4</sub>/REO interfaces using high-resolution Z-contrast imaging and electron-energy-loss spectroscopy (EELS) in the scanning transmission electron microscope (STEM) clearly stand out due to the important new information they have provided on the atomic and electronic structures of the ceramic.<sup>3–11</sup>

Based on the recent STEM experiments from various groups, it is now well known that the structure of the IGF formed by the REO has a partial ordering with the rare-earth elements arranged periodically at the interface. Atomic-scale information on the position and local concentration of the interfacial oxygen, on the other hand, is just beginning to emerge. Earlier, Ziegler *et al.*<sup>4</sup> correlated the particular bonding patterns of the various rare-earth elements with their atomic size and electronic configuration, as well as the presence of interfacial oxygen, which was inferred indirectly from comparisons of the EELS results for the Si *L*<sub>2,3</sub> edges with reference spectra. In a very recent experimental study in which we obtained oxygen *K* as well as cerium *M* edges at a

Si<sub>3</sub>N<sub>4</sub>/CeO<sub>2- $\delta$</sub>  interface, we provided conclusive evidence for the presence of oxygen at the interface.<sup>11</sup> Furthermore, our experiments suggested that the characteristic open rings in the contact layer of the Si<sub>3</sub>N<sub>4</sub> matrix grains were most likely oxygen terminated as the onset of the O signal was measured to occur  $\sim 2$  Å before the Ce signal in going from the grain to the IGF.

As for theoretical investigations on the surface and interfacial properties of  $\beta$ -Si<sub>3</sub>N<sub>4</sub>, in earlier studies researchers have typically employed empirical methods such as those based on tight binding or pair potentials.<sup>12</sup> Recently, computational studies using first-principles techniques have become more feasible and popular. For example, Painter *et al.*<sup>13</sup> used a differential binding-energy approach to study rare-earth effects on grain growth and microstructure in  $\beta$ -Si<sub>3</sub>N<sub>4</sub> ceramics, while Rulis *et al.*<sup>14</sup> used a combination of classical molecular-dynamics simulations and first-principles methods to model the IGF between  $\beta$ -Si<sub>3</sub>N<sub>4</sub> (0001) surfaces. The electronic structure of the bare (0001) basal surface and how oxygen adsorbs on it were also recently studied by Bermudez<sup>15</sup> and Wang *et al.*,<sup>16</sup> respectively. Finally, in combined experimental and theoretical studies, Shibata and co-workers<sup>3,6,8</sup> examined the adsorption sites and structural energetics of La, Gd, and Lu on the prismatic planes of  $\beta$ -Si<sub>3</sub>N<sub>4</sub>. However, in their work Shibata *et al.* assumed the rare-earth element to be in direct contact with the nitrogen-terminated Si<sub>3</sub>N<sub>4</sub> (10 $\bar{1}$ 0) surface without consideration for oxygen termination.

In addition to the computational work mentioned above, a few years ago some of the present authors started a systematic *ab initio* study of the Si<sub>3</sub>N<sub>4</sub>/REO interface by investigating the atomic and electronic structures of various *bare*  $\beta$ -Si<sub>3</sub>N<sub>4</sub> surfaces.<sup>17</sup> In that work, Idrobo *et al.* showed that the stoichiometric open-ring termination of  $\beta$ -Si<sub>3</sub>N<sub>4</sub> (10 $\bar{1}$ 0), which has been consistently observed in the recent STEM experiments, was, in fact, higher in energy than other stoichiometric as well as nonstoichiometric terminations. Based on this somewhat puzzling result obtained for the bare surface, the authors argued that oxygen, rare-earth elements, and/or the other sintering additives must have been changing

the relative stability of the prismatic plane terminations in  $\text{Si}_3\text{N}_4$ . Motivated by this plausible suggestion as well as by our recent experimental results which indicate the presence of interfacial oxygen, in this paper, we continue with our *ab initio* studies of the interface by focusing on the structural energetics of oxygen adsorption on  $\beta\text{-Si}_3\text{N}_4$  ( $10\bar{1}0$ ) surfaces. We consider a large pool of initial structures corresponding to various stoichiometric and nonstoichiometric surface configurations with and without surface reconstructions and identify the lowest-energy structures at four different coverages. We show that oxygen has a strong tendency to replace nitrogen in a bridging configuration between two Si atoms. We predict that most of the oxygenated low-energy surfaces are nonstoichiometric and have  $(1 \times 2)$  reconstructions. We identify energetically most favorable oxygen coverages and discuss the implications of our findings in light of the experimental results and our previous computations on the bare surface. The rest of the paper is organized as follows. In Sec. II, we present the computational methods and parameters. The lowest-energy structures at different coverages, along with a discussion of their relative stability as a function of stoichiometry, are presented in Sec. III. We conclude with a brief summary in Sec. IV.

## II. COMPUTATIONAL METHODS AND PARAMETERS

All calculations were performed within the framework of density-functional theory using the projector augmented wave method as implemented in VASP.<sup>18</sup> For exchange correlation, we used the Perdew-Wang (PW) parametrization<sup>19</sup> of the generalized gradient approximation (GGA). For the low-energy structures obtained, we repeated the computations using the Perdew-Burke-Ernzerhof (PBE) (Ref. 20) parametrization of GGA. We observed that the total-energy differences between different structures were quite insensitive to the choice of the exchange-correlation functional (PW versus PBE) remaining within less than 0.1 eV of each other. The hexagonal bulk unit cell of  $\beta\text{-Si}_3\text{N}_4$  contains 14 atoms and six structural parameters:  $a$ ,  $c$ , and four internal parameters. The surface calculations were performed using the theoretical structural parameters  $(a, c, x_{\text{Si}}, y_{\text{Si}}, x_{\text{N}}, y_{\text{N}}) = (7.667 \text{ \AA}, 2.928 \text{ \AA}, 0.1752, 0.7692, 0.3299, 0.031)$ , which are in good agreement with the experimental values of  $(7.608 \text{ \AA}, 2.911 \text{ \AA}, 0.1733, 0.7694, 0.3323, 0.0314)$ .

Our previous convergence tests for surface energies<sup>17</sup> showed that the  $(10\bar{1}0)$  surface of  $\beta\text{-Si}_3\text{N}_4$  can be modeled accurately with a *symmetric* five-layer slab (with equivalent top and bottom surfaces) and a vacuum region of 10  $\text{\AA}$ . Since we performed a large number of first-principles structural optimization computations at various coverages for the different initial adsorbate positions (approximately 350 different starting configurations), we reduced the computational demand by working with *asymmetric* three-layer slabs, in which the atoms of the bottom unit cell were fixed at their bulk positions and their dangling bonds were passivated by hydrogens. Such asymmetric three-layer slabs model the  $(10\bar{1}0)$  surface quite well as we found the binding energies (BEs) calculated with symmetric versus asymmetric slabs to

be within less than 0.1 eV of each other. Still, in order to ensure accuracy of the final results, for low-energy configurations found at each coverage (approximately ten configurations), we repeated the computations with seven-layer symmetric slabs and the vacuum size increased to 14  $\text{\AA}$ , which are reported here. The  $(1 \times 1)$  unit cell of the  $(10\bar{1}0)$  surface of  $\beta\text{-Si}_3\text{N}_4$  has dimensions of  $a \times c$ . Dictated by the coverages we investigated and taking into account possible reconstructions, we also considered  $(1 \times 2)$  surface unit cells (doubled along the  $c$  direction). In all computations, we used an energy cutoff of 270 eV and a  $1 \times 3 \times 8$  Monkhorst-Pack grid (for a  $1 \times 1$  surface unit cell) for  $\mathbf{k}$ -point sampling, which have been shown in our previous studies to provide well-converged structural energetics.

## III. RESULTS AND DISCUSSION

Before we examine the low-energy configurations of oxygen on the  $\text{Si}_3\text{N}_4$  ( $10\bar{1}0$ ) surface at various coverages, we briefly summarize our earlier findings regarding the nature of the atomic relaxations and structural energetics of the bare (oxygen-free) stoichiometric  $\text{Si}_3\text{N}_4$  ( $10\bar{1}0$ ) surface. There are two different stoichiometric terminations of the  $\text{Si}_3\text{N}_4$  ( $10\bar{1}0$ ) surface; the open-ring and the “closed-ring” (referred to as “half surface” in Ref. 17) surfaces as shown in Fig. 1(a). On the unrelaxed open-ring surface, there are one Si and one N atom, which have one dangling bond each. These are represented by Si2 and N1 in Fig. 1(a). Upon relaxation [Fig. 1(b)], Si2 undergoes a large relaxation ( $\sim 0.8 \text{ \AA}$ ) and forms a new Si-Si bond (at 2.58  $\text{\AA}$ ) with Si4. As a result, the dangling bond of Si2 is saturated (at the expense of overcoordination of Si4 with two resonant bonds), while N1 still remains with a dangling bond. On the unrelaxed closed-ring surface, there are also one Si atom (Si4) and one N atom (N5), both of which have one dangling bond. When relaxed [Fig. 1(c)], Si4 moves inward considerably (by  $\sim 0.64 \text{ \AA}$ ) and achieves an  $sp^2$ -type bonding in a nearly planar configuration with three N atoms. Total-energy calculations with PW or PBE exchange-correlation functionals indicate that the relaxed closed-ring surface is 0.17 eV (per  $1 \times 1$  surface unit cell) lower in energy than the relaxed open-ring surface, which has been consistently observed in all recent STEM experiments at the REO interfaces. This has suggested that oxygen, the rare-earth elements and/or other sintering additives most likely change the relative stability of the terminations of  $\beta\text{-Si}_3\text{N}_4$  surfaces.

As mentioned above, the unrelaxed  $(10\bar{1}0)$  surfaces (open-ring or closed-ring) exhibit two dangling bonds per  $(1 \times 1)$  surface unit cell. Based on this, we define a 1 monolayer (ML) oxygen coverage ( $\Theta = 1 \text{ ML}$ ) as a configuration in which two oxygen atoms per  $(1 \times 1)$  unit cell are present on the  $(10\bar{1}0)$  surface. In our study, we considered oxygen coverages of  $\Theta = \frac{1}{4}, \frac{1}{2}, \frac{3}{4}$ , and 1 ML and surface unit cells of  $(1 \times 1)$  and  $(1 \times 2)$ . Using these cells,  $\frac{1}{4}$  and  $\frac{3}{4}$  ML coverages can only be achieved with  $(1 \times 2)$  unit cells, while  $\frac{1}{2}$  and 1 ML coverages can be obtained with reconstructed  $(1 \times 2)$  cells or can be constrained to  $(1 \times 1)$  surface unit cells. Be-

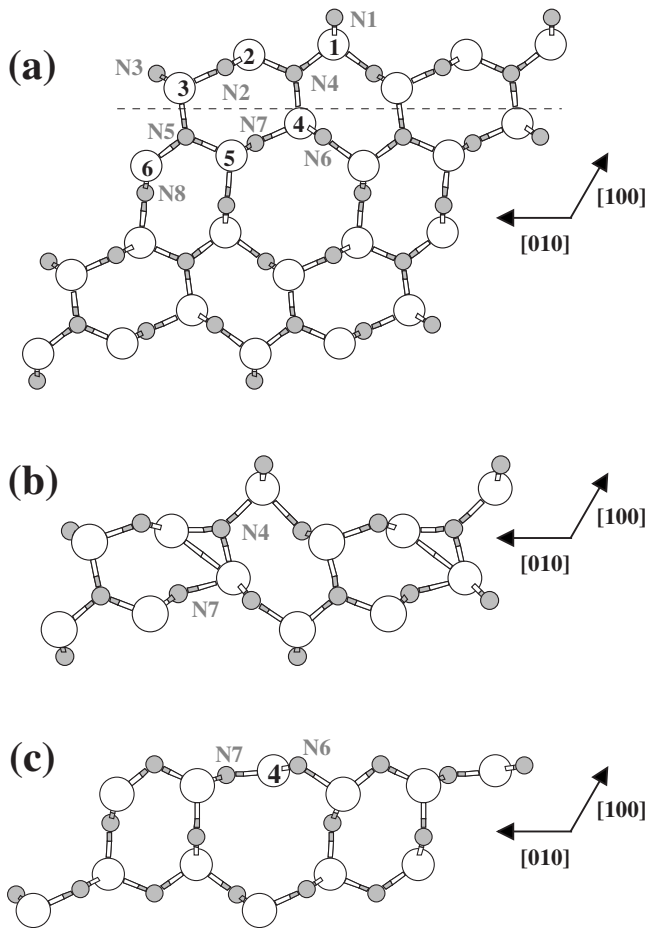


FIG. 1. (a) [001] projected double-unit-cell view of a two-layer unrelaxed  $(10\bar{1}0)$  bare open-ring surface. If the atoms above the dashed line are removed, the unrelaxed closed-ring surface is obtained. (b) and (c) show the [001] projected double-unit-cell views of the top-layers of the relaxed open-ring and closed-ring surfaces, respectively. The indices for the N atoms (gray circles) are given in gray next to them and the indices for the Si atoms (white circles) are shown inside the white circles. For example, the index 1 inside a white circle denotes the Si1 atom mentioned in the text.

low, we examine the low-energy configurations which resulted from our studies at each coverage.

#### A. $\Theta = \frac{1}{4}$ ML coverage

The two most stable configurations corresponding to the  $\Theta = \frac{1}{4}$  ML coverage are shown in Fig. 2. For the open-ring configuration [Fig. 2(a)], one O replaces every second N atom (N1 in Fig. 1), which connects the Si atoms in a zigzag chain along the [001] direction. The replaced N, in turn, bridges two Si atoms (Si2 in Fig. 1), thus saturating their dangling bonds. This N atom also forms a bond along the [010] direction (parallel to the surface along the  $a$  axis) with the N atom positioned in between the bridging O. Ideally, as in bulk silicon oxynitride ( $\text{Si}_2\text{N}_2\text{O}$ ), Si, N, and O atoms would prefer to be fourfold, threefold, and twofold coordinated, respectively. Indeed, the relatively high BE, which we found to be 4.83 eV per O atom (referenced to molecular

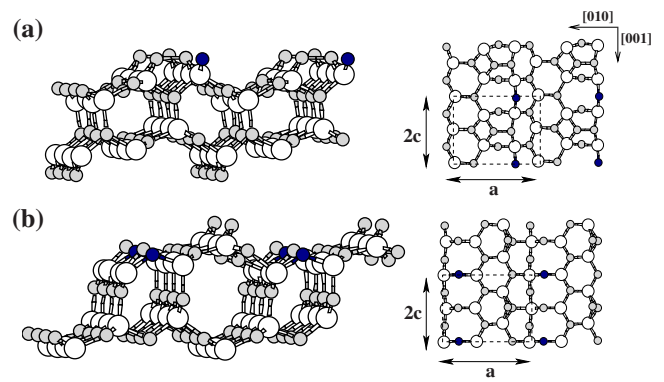


FIG. 2. (Color online) (a) Oblique (slightly off the [001] projection) and extended (surface unit cell doubled along [010] and [001] directions) view of the lowest-energy open-ring configuration at  $\Theta = \frac{1}{4}$  ML oxygen coverage. On the right, a top view is provided showing the surface unit cell with a dashed rectangle. (b) The same for the lowest-energy closed-ring configuration. The oxygen atoms are shown with blue (dark) circles.

oxygen) for the open-ring configuration at  $\Theta = \frac{1}{4}$  ML, is due to the fact that all atoms in this structure are ideally coordinated without any dangling bonds or overcoordination.

A similar bridging oxygen (Si-O-Si) bonding pattern occurs for the most stable closed-ring configuration as shown in Fig. 2(b). In this case, the O atom similarly replaces every second N atom with a dangling bond (N5 in Fig. 1), and the replaced N forms two bonds with the Si atoms (Si4 in Fig. 1), thus saturating their dangling bonds. However, unlike the open-ring structure this closed-ring configuration does not result in an ideal coordination for all atoms since two N atoms per  $(1 \times 2)$  cell remain with a dangling bond each. As a result, the closed-ring surface at  $\Theta = \frac{1}{4}$  ML oxygen coverage is energetically less stable than the open-ring surface, as the BE per O atom drops by 0.90 eV to 3.93 eV. These observations show that it is indeed possible for the relative stability of two different surface terminations to change upon oxygenation, which might provide the answer for why the open-ring termination has been consistently observed at the  $\text{Si}_3\text{N}_4/\text{REO}$  interfaces.

#### B. $\Theta = \frac{1}{2}$ ML coverage

The characteristic Si-O-Si bridging oxygen configuration, resulting from the replacement of a surface N atom with O, is also observed for the most stable  $\Theta = \frac{1}{2}$  ML stoichiometric configurations. If we constrain our search at this coverage to  $(1 \times 1)$  surfaces (corresponding to one O atom in the unit cell), we find that the lowest-energy open-ring configuration is the structure shown in Fig. 3(a), which has one overcoordinated Si atom (Si2) and one N atom (bonded with two Si2 atoms) with a dangling bond. The calculated BE per O atom for this configuration is 3.06 eV. We note that while both O and N atoms connect Si atoms in a zigzag fashion along [001], their particular positions in the unit cell are crucial. Namely, O connects Si1-type atoms which are connected to two subsurface nitrogen atoms (N3 and N4 in Fig. 1), while the N bridges overcoordinated Si2-type atoms which are

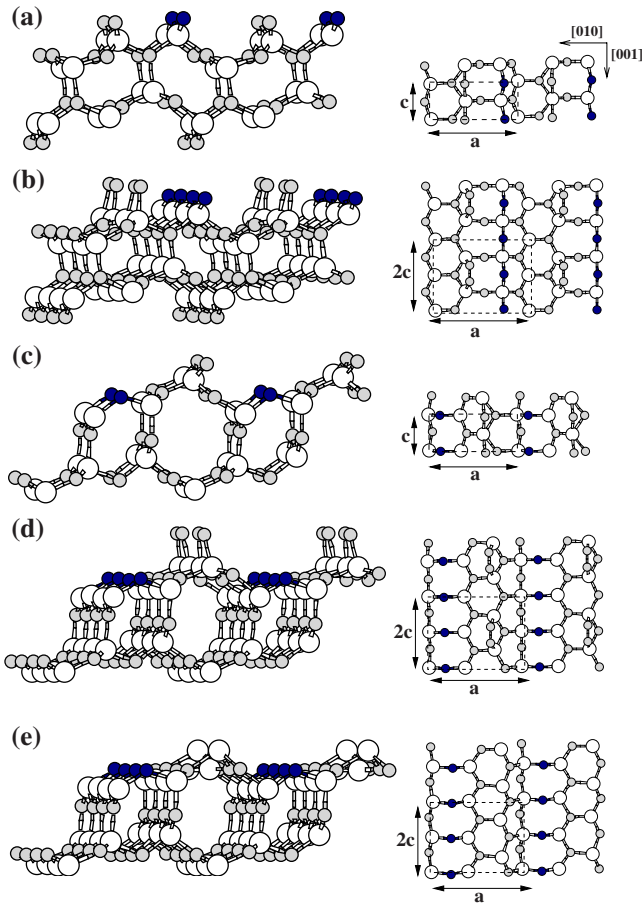


FIG. 3. (Color online) (a) Oblique (slightly off the [001] projection) and extended (surface unit cell doubled along [010] and [001] directions) view of the lowest-energy unreconstructed open-ring configuration at  $\Theta = \frac{1}{2}$  ML oxygen coverage. On the right, a top view is provided showing the surface unit cell with a dashed rectangle. (b), (c), and (d) show the same for the  $(1 \times 2)$  reconstructed open-ring surface, the unreconstructed closed-ring surface, and  $(1 \times 2)$  reconstructed closed-ring surface, respectively. (e) A low-energy, nonstoichiometric [with two N atoms missing per  $(1 \times 2)$  cell], and reconstructed closed-ring configuration. The oxygen atoms are shown with blue (dark) circles.

connected to three subsurface nitrogen atoms (in Fig. 1, these are N4 and two N2 atoms in neighboring unit cells separated by  $c$ ). If the positions of O and N were switched, which would result in Si1-N-Si1 and Si2-O-Si2 zigzag chains, Si2 atoms would be overcoordinated with three N and two O atoms [as opposed to five N atoms, as shown in Fig. 3(a)], and the BE per O atom for the relaxed structure would drop to 2.28 eV. This is an example of a general trend we observed in the structural energetics of oxygenated  $\text{Si}_3\text{N}_4$  surfaces, namely, fivefold coordinated Si is not necessarily energetically too costly, especially if the resonant bonds of the corresponding configuration are with two N atoms rather than O.

If we allow for the possibility of a  $(1 \times 2)$  surface reconstruction at  $\Theta = \frac{1}{2}$  ML oxygen coverage, we obtain an energetically more favorable open-ring configuration [Fig. 3(b)] than the  $(1 \times 1)$  structure discussed above. The reconstructed surface is similar to the unreconstructed one: The oxygen

atoms still form Si2-O-Si2 zigzag chains along [001], however, the nitrogen atoms attached to Si1 type surface atoms now form dimers. While both N atoms in the dimer still have one dangling bond each (as in the unreconstructed surface), the main effect of the dimerization is to prevent overcoordination of Si1 type atoms, which are now ideally fourfold coordinated. As a result of this  $(1 \times 2)$  reconstruction, the BE per O atom increases to 4.38 eV, which is 1.32 eV larger than the value calculated for the lowest-energy unreconstructed configuration [Fig. 3(a)] found at this coverage. This shows one example of the several oxygen-induced reconstructions on  $\beta\text{-Si}_3\text{N}_4$  (10 $\bar{1}0$ ) surfaces we observed during the course of our studies.

A similar surface reconstruction occurs for the closed-ring configurations. Figure 3(c) shows the most stable  $(1 \times 1)$  closed-ring structure at  $\Theta = \frac{1}{2}$  ML coverage. O atom again replaces the N atom (N5) with a dangling bond on the unreconstructed closed-ring surface, and each replaced N is attached to two Si atoms (Si4 type with one initial dangling bond) and overcoordinates the latter. The bridging Si-O-Si configuration along the  $a$  direction (i.e., [010]) is locally quite stable and is observed in all lowest-energy closed-ring configurations. The BE per O atom for this structure is 3.31 eV, which is larger than that of the  $(1 \times 1)$  open-ring configuration. Further gain in the BE can be achieved by allowing a  $(1 \times 2)$  reconstruction, as shown in Fig. 3(d). This structure is again similar to the unreconstructed one in Fig. 3(c) except that the Si4 atoms are now ideally (fourfold) coordinated, and the N atoms attached to them dimerize along [001] to reduce the number of their dangling bonds. This simple reconstruction caused by the dimerization of the N atoms gives rise to a large energy gain of 1.35 eV resulting in a BE of 4.66 eV per O atom.

So far we have presented several examples which show that O has a rather strong tendency to replace N substitutionally rather than to attach to the surface epitaxially or interstitially. In most cases, the replaced N stays on the surface and typically helps saturate dangling Si bonds. In some cases, however, we observed that the N atoms would form dimers and diffuse away from the surface into the vacuum region, while the rest of the system was structurally optimized. Such behavior suggested that substoichiometry on the N sublattice could potentially play an important role in the stability of oxygenated  $\beta\text{-Si}_3\text{N}_4$  surfaces. Pursuant to these observations, we extended our search to nonstoichiometric surfaces by recalculating total energies with such N dimers removed, as well as trying new N-deficient initial structures (based on general bonding trends and minimization of dangling bonds) that could potentially yield low-energy structures. As will be shown later, when the total energies of such nonstoichiometric structures are compared with those of stoichiometric ones using the allowed ranges of the chemical potentials involved, we find that most of the lowest-energy structures that appear in the phase diagram of O/ $\text{Si}_3\text{N}_4$  are indeed nonstoichiometric. An example of a low-energy nonstoichiometric surface at  $\Theta = \frac{1}{2}$  is shown in Fig. 3(e). The starting point for this optimized structure is the  $(1 \times 2)$  closed-ring configuration discussed above [Fig. 3(d)] with the N dimers removed. Although one might think that the

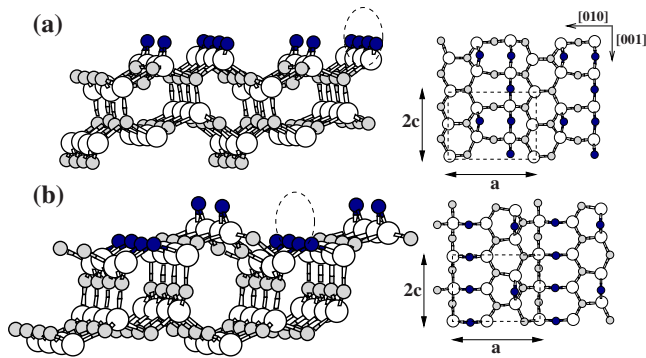


FIG. 4. (Color online) (a) Oblique (slightly off the  $[001]$  projection) and extended (surface unit cell doubled along  $[010]$  and  $[001]$  directions) view of the lowest-energy open-ring configuration at  $\Theta = \frac{3}{4}$  ML oxygen coverage. On the right, a top view is provided showing the surface unit cell with a dashed rectangle. (b) The same for the lowest-energy closed-ring configuration. The oxygen atoms are shown with blue (dark) circles. The dashed ellipses show the Si-O-Si bridges mentioned in the text.

reconstruction induced by the N dimers would disappear when they are removed, symmetry-unrestricted reoptimization of the structure yields a new  $(1 \times 2)$  reconstruction. The reconstruction is now due to alternating positions of the two neighboring Si4-type atoms along the  $[001]$  direction. When the N dimer is removed, one of the Si4 atoms remains with a dangling bond, as in the *unrelaxed* bare closed-ring surface shown in Fig. 1(a), while the other moves toward the surface and exhibits an  $sp^2$ -type bonding in a nearly planar configuration with three N, as in the *relaxed* bare closed-ring surface shown in Fig. 1(c). In addition, in spite of the significant distortion due to the Si4 atom, both N6-type nitrogen atoms (in neighboring unit cells along  $[001]$ ) keep their preferred nearly planar coordination with three Si atoms. Since this structure is nonstoichiometric, it is not straightforward to compare the BE per O atom for this configuration with those for the stoichiometric ones even at the same coverage. For the moment, we note that (as will be shown in Sec. III E) this rather peculiar structure with one Si dangling bond and no N dangling bonds is indeed one of the lowest-energy structures in the N-poor region of the phase diagram. It is also one of the two low-energy structures (out of approximately 350 structures we considered), in which the dangling bond of a Si atom has *not* been saturated via  $sp^2$  or overcoordinated resonant bond distortions or by achieving the ideal  $sp^3$  configuration by N or O attachment.

### C. $\Theta = \frac{3}{4}$ ML coverage

From a large pool of stoichiometric and nonstoichiometric structures investigated at the  $\Theta = \frac{3}{4}$  ML oxygen coverage (corresponding to 3 O atoms on  $1 \times 2$  surfaces), the structures shown in Figs. 4(a) and 4(b) are by far the most stable open-ring and closed-ring configurations, respectively. Both structures are nonstoichiometric with two N atoms per  $(1 \times 2)$  cell missing. The two-thirds ratio between the number of missing N atoms (nominally in the  $-3$  charge state) and the number of added O atoms (nominally in the  $-2$  charge

state) is crucial for the enhanced stability of these surfaces, which results in no dangling bonds or overcoordinated atoms. In fact, it is possible to predict, based on the general bonding trends observed so far, that the structures shown in Figs. 4(a) and 4(b) are likely to be quite stable. For example, for the open-ring surfaces, we have already seen several examples where it is energetically favorable for O to replace the N1-type atoms and bridge the Si1 atoms. This requires two O atoms and results in two missing N atoms per  $(1 \times 2)$  cell. These N atoms, for stoichiometric surfaces, would typically bond to Si2 atoms, but this results in overcoordination of Si2 [Fig. 3(a)] or dangling N bonds [Fig. 3(b)]. Instead, if these two N atoms are removed from the surface and the third O is used to saturate the dangling Si2 bond (fully saturating both Si2 and O bonds), the resulting structure, as shown in Fig. 4(a) after structural optimization, is expected to be quite stable. Similarly for the closed-ring configuration, we have seen that it is energetically favorable for O to replace the N5 type atoms and bridge two Si atoms (Si5 and Si6 in Fig. 1) resulting in a Si-O-Si bridge along the  $a$  direction. If this is done for two  $(1 \times 1)$  unit cells (two added O and two removed N atoms) in addition to saturating the Si4 dangling bonds with a third O atom (thereby saturating both bonds of the added oxygen), the resulting structure, as shown in Fig. 4(b) after structural optimization, is expected to be quite stable. As will be shown in Sec. III E, this is indeed the case as this structure stands out as the lowest-energy structure for a large portion of the calculated phase diagram.

The local environments for O in the two most stable structures at  $\Theta = \frac{3}{4}$  ML coverage, shown in Figs. 4(a) and 4(b), are similar. In spite of the similarities, we find that the closed-ring surface is lower in energy by 0.56 eV per  $(1 \times 2)$  cell than the open-ring structure. To understand this, we first note that the local environments around the oxygens saturating the Si2 and Si4 atoms in Figs. 4(a) and 4(b), respectively, are almost identical. As such, it is natural to attribute the energetic favorability of the closed-ring configuration to the differences in the geometric constraints imposed on the Si-O-Si bridges, shown by dashed ellipses in Figs. 4(a) and 4(b). In particular, the distance between Si5 and Si6 along the  $a$  direction is  $\sim 0.1$  Å larger than the Si1-Si1 separation (i.e., the lattice parameter  $c$ ) along the  $[001]$  direction. This extra room allows the Si atoms bonded to the bridging O in the closed-ring configuration to achieve nearly perfect tetrahedral coordination (with the bridging O and three N atoms) while still maintaining a large Si-O-Si bond angle of  $\sim 129^\circ$ , close to the  $142^\circ$  bond angle observed in bulk  $\text{SiO}_2$ . In the open-ring configuration, on the other hand, the relaxed Si1-O-Si1 bond angle is only  $121^\circ$ , significantly smaller than the preferred bulk value. The reason that this angle cannot be made larger (with the O relaxing more inward, for example) is that such a configuration would cost more energy overall since it would considerably distort the nearly tetrahedral coordination of the Si1 atoms. As such, the energetic favorability of the closed-ring configuration results from the delicate balance it can sustain between the tetrahedral bonding angle of Si and the bridging angle of O between two Si atoms in this strongly covalent material.

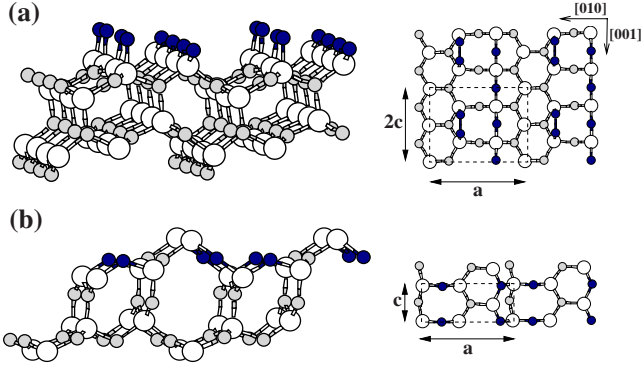


FIG. 5. (Color online) (a) Oblique (slightly off the  $[001]$  projection) and extended (surface unit cell doubled along  $[010]$  and  $[001]$  directions) view of a low-energy  $(1 \times 2)$  reconstructed and nonstoichiometric [with two N atoms missing per  $(1 \times 2)$  surface cell] open-ring configuration at  $\Theta = 1$  ML oxygen coverage. On the right, a top view is provided showing the surface unit cell with a dashed rectangle. (b) The same for a low-energy, unreconstructed, and nonstoichiometric [with two N atoms missing per  $(1 \times 1)$  surface cell] closed-ring configuration. The oxygen atoms are shown with blue (dark) circles.

#### D. $\Theta = 1$ ML coverage

Since the  $\Theta = 1$  ML coverage can be achieved in two ways [two oxygens on  $(1 \times 1)$  or four oxygens on reconstructed  $(1 \times 2)$  surface cells] and there are more possibilities for the relative positioning of the oxygen atoms on the surface, we explored a large number of configurations at this coverage. As expected, most of the low-energy surfaces turned out to be N-deficient nonstoichiometric structures. Two of them are shown in Figs. 5(a) and 5(b). The open-ring configuration shown in Fig. 5(a) is fully oxygenated and has a  $(1 \times 2)$  surface reconstruction induced by the dimerization of oxygens which saturate the dangling bonds of Si2-type atoms. As in most low-energy open-ring structures, the N atoms connecting Si1 chains along  $[001]$  have been replaced by O atoms, resulting in two missing N atoms per  $(1 \times 2)$  surface unit cell. The closed-ring configuration, shown in Fig. 5(b), is also nonstoichiometric with two N atoms missing per  $(1 \times 1)$  cell, but it does not have a surface reconstruction. Reminiscent of the structure shown in Fig. 3(e), Si4 atom has a dangling bond as in the unrelaxed bare closed-ring surface and the O atoms connected to Si4 are overcoordinated in a nearly planar configuration with three Si atoms. In spite of these peculiar features, this closed-ring configuration can be competitive in energy in the N-poor region of the phase diagram, as will be discussed next.

#### E. Phase diagram of $\beta$ -Si<sub>3</sub>N<sub>4</sub> ( $10\bar{1}0$ ) surface

We now compare the total energies of all low-energy surfaces with different amounts of oxygen coverage and nitrogen stoichiometry. The total energy for a given surface configuration can be written as<sup>21</sup>

$$E_{\text{surface}} = E_{\text{slab}} - n_{\text{Si}}\mu_{\text{Si}} - n_{\text{N}}\mu_{\text{N}} - n_{\text{O}}\mu_{\text{O}}, \quad (1)$$

where  $E_{\text{slab}}$  is the total energy of the corresponding slab,  $n_i$  is the number of atoms of type  $i$  in the slab, and  $\mu_i$ 's are the

TABLE I. The coverage ( $\Theta$ ), the figure label, and the total energy per  $(1 \times 1)$  unit cell (referenced to the bare open-ring surface) of all the low-energy oxygen configurations on the  $\beta$ -Si<sub>3</sub>N<sub>4</sub> ( $10\bar{1}0$ ) surfaces discussed in the text. To obtain the total energies referenced to the lower-energy bare closed-ring surface (which are used to produce the phase diagram in Fig. 6), 0.17 eV should be added to the energies reported below. The number of dangling bonds ( $N_{\text{db}}$ ) and the number of overcoordinated atoms ( $N_{\text{oc}}$ ) per  $(1 \times 1)$  cell are also provided. The letter  $R$  next to some of the figure labels in the second column indicates that the surface has a  $(1 \times 2)$  reconstruction.

$\Theta$	Figure	Total energy (eV)	$N_{\text{db}}$	$N_{\text{oc}}$
$\frac{1}{4}$	2(a)	$-4.69 - \frac{1}{2}\mu_{\text{O}}$		
	2(b)	$-4.24 - \frac{1}{2}\mu_{\text{O}}$	1	
$\frac{1}{2}$	3(a)	$-7.60 - \mu_{\text{O}}$	1	1
	3(b)-R	$-8.92 - \mu_{\text{O}}$	1	
	3(c)	$-7.85 - \mu_{\text{O}}$	1	1
	3(d)-R	$-9.20 - \mu_{\text{O}}$	1	
	3(e)-R	$-0.63 - \mu_{\text{O}} + \mu_{\text{N}}$	1	
$\frac{3}{4}$	4(a)	$-5.00 - \frac{3}{2}\mu_{\text{O}} + \mu_{\text{N}}$		
	4(b)	$-5.28 - \frac{3}{2}\mu_{\text{O}} + \mu_{\text{N}}$		
1	5(a)-R	$-7.84 - 2\mu_{\text{O}} + \mu_{\text{N}}$		
	5(b)	$0.75 - 2\mu_{\text{O}} + 2\mu_{\text{N}}$	1	1

corresponding chemical potentials, which satisfy  $3\mu_{\text{Si}} + 4\mu_{\text{N}} = \mu_{\text{Si}_3\text{N}_4, \text{bulk}}$ . From the upper limits on the N and Si chemical potentials ( $\mu_{\text{Si}} \leq \mu_{\text{Si}, \text{bulk}}$  and  $\mu_{\text{N}} \leq \frac{1}{2}\mu_{\text{N}_2}$ ) we find the allowed range of  $\mu_{\text{N}}$  to be  $-10.29 \leq \mu_{\text{N}} \leq -7.67$  eV. The upper limit for the oxygen chemical potential can be made more strict than the condition given by  $\mu_{\text{O}} \leq \frac{1}{2}\mu_{\text{O}_2} = -4.56$  eV (PW) by preventing the precipitation of bulk Si<sub>2</sub>N<sub>2</sub>O, namely  $2\mu_{\text{Si}} + 2\mu_{\text{N}} + \mu_{\text{O}} \leq \mu_{\text{Si}_2\text{N}_2\text{O}, \text{bulk}}$ . Combining this criterion with the condition of equilibrium with bulk Si<sub>3</sub>N<sub>4</sub>, we get the condition  $\mu_{\text{O}} - \frac{2}{3}\mu_{\text{N}} \leq -2.48$  eV, which limits the maximum of the oxygen chemical potential to  $-9.34$  (N-poor region) and  $-7.59$  eV (N-rich region).

Table I shows the total-energy expressions per  $(1 \times 1)$  surface unit cell for all surface configurations at different coverages discussed so far as a function of the oxygen and nitrogen chemical potentials. Although it is not the lowest-energy bare surface, since the open-ring configuration is the one observed at the REO interfaces, we have referenced all surface total energies with respect to the bare open-ring surface (a negative surface total energy at a given  $\mu_{\text{O}}$  and/or  $\mu_{\text{N}}$  means that it is energetically more favorable for that surface to form under those conditions compared to the bare open-ring surface). The table also provides a summary of the number of dangling bonds and the number of overcoordinated atoms per  $(1 \times 1)$  cell.

Based on the calculated energies, we show in Fig. 6 the zero-temperature phase diagram of the oxygenated  $\beta$ -Si<sub>3</sub>N<sub>4</sub> ( $10\bar{1}0$ ) surface as a function of  $\mu_{\text{N}}$  and  $\mu_{\text{O}}$ . In the allowed ranges of the chemical potentials, there are three oxygenated lowest-energy structures, shown in Figs. 3(d), 3(e), and 4(b).

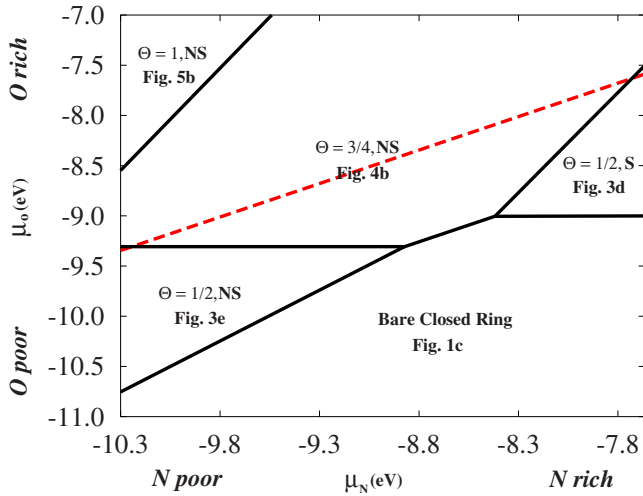


FIG. 6. (Color online) The zero-temperature phase diagram of the oxygenated  $\beta$ - $\text{Si}_3\text{N}_4$  ( $10\bar{1}0$ ) surface as a function of the N and O chemical potentials showing the lowest-energy structures, their corresponding oxygen coverages and figure labels, and whether they are stoichiometric (S) or nonstoichiometric (NS). The dashed line shows the saturation condition with bulk  $\text{Si}_2\text{N}_2\text{O}$ , i.e.,  $\mu_{\text{O}} - \frac{2}{3}\mu_{\text{N}} = -2.48$  eV, as discussed in the text. The region of the phase space above this line would favor the formation of bulk  $\text{Si}_2\text{N}_2\text{O}$ .

The structure displayed in Fig. 5(b) also appears as the lowest-energy structure under O-rich and N-poor conditions, but this region should be excluded as it would favor the formation of bulk  $\text{Si}_2\text{N}_2\text{O}$ . Nonstoichiometry (arising from N deficiency) plays an important role in the structural energetics, as mentioned before, with three of the four lowest-energy surfaces shown in Fig. 6 corresponding to nonstoichiometric surfaces. It is also interesting to note that all the lowest-energy surfaces are based on the closed-ring configuration. A large portion of the phase diagram is occupied by the closed-ring configuration at  $\Theta = \frac{3}{4}$  ML oxygen coverage, shown in Fig. 4(b). In fact, when  $\mu_{\text{O}}$  achieves its maximum value (just before the formation of bulk  $\text{Si}_2\text{N}_2\text{O}$ ), this configuration is the lowest-energy structure among all structures for almost the entire range of the N chemical potential.

As discussed above, the phase diagram shown in Fig. 6 shows the lowest-energy structure at given values of the O and N chemical potentials. In most cases, many low-energy structures compete with the lowest-energy structure. In order to show the richness in the structural energetics of the  $\beta$ - $\text{Si}_3\text{N}_4$  ( $10\bar{1}0$ ) surface, we also plot in Fig. 7 the energies of the various surfaces shown in Figs. 2–5 as a function of  $\mu_{\text{O}}$  at three different values of  $\mu_{\text{N}}$  corresponding to N-poor, N-rich, and intermediate N stoichiometries. The figure shows that the closed-ring  $\Theta = \frac{3}{4}$  structure is quite low in energy even when it is not the lowest-energy structure [Figs. 7(a) and 7(b)]. We also observe that of all the open-ring configurations, the one that is the most competitive in energy with closed-ring configurations is the  $\Theta = \frac{1}{4}$  ML structure [Fig. 2(a)], as shown in Fig. 7(b). If we focus on the maximum solubility limit of oxygen, as shown by the dashed line in Fig. 6, the corresponding coverage is  $\Theta = \frac{3}{4}$  ML and the most stable surface has a closed-ring configuration which is now

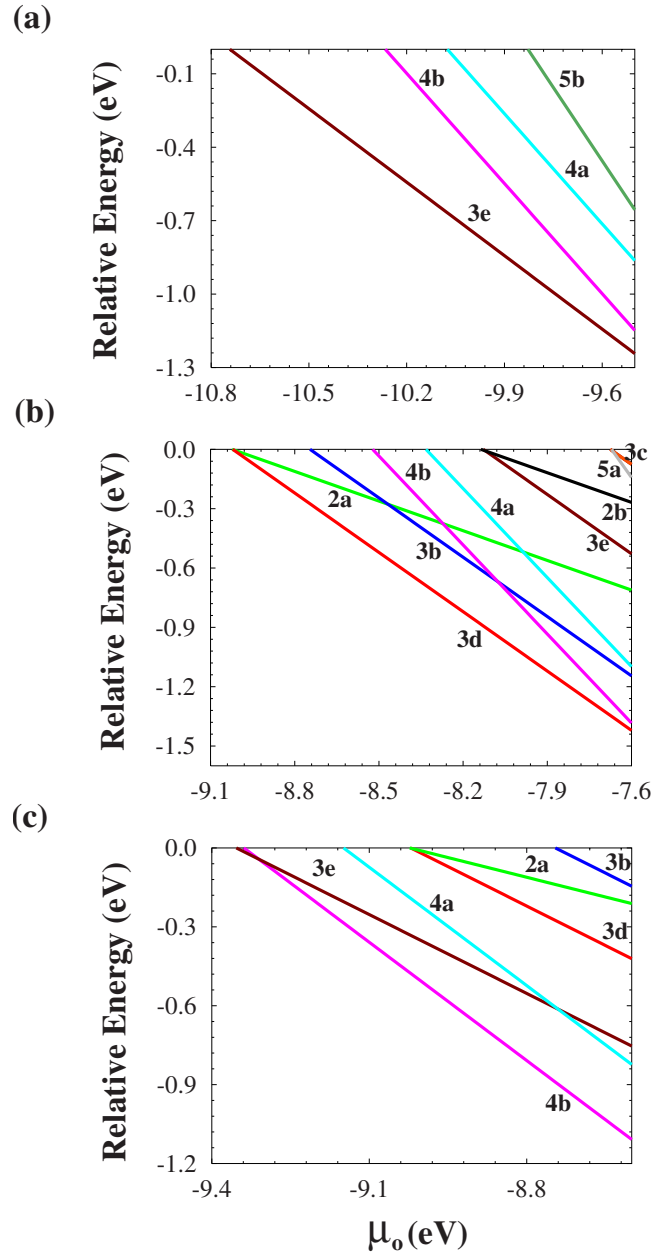


FIG. 7. (Color online) The formation energies (relative to the bare closed-ring configuration) of various surfaces discussed in the text (as shown with their figure labels) as a function of the O chemical potential  $\mu_{\text{O}}$  at three different N chemical potential values corresponding to (a)  $\mu_{\text{N}} = -10.29$  eV (N-poor), (b)  $\mu_{\text{N}} = -7.67$  eV (N-rich), and (c)  $\mu_{\text{N}} = -8.90$  eV (intermediate N-stoichiometry) conditions. At each value of  $\mu_{\text{N}}$ , the largest  $\mu_{\text{O}}$  value is dictated by preventing precipitation of bulk  $\text{Si}_2\text{N}_2\text{O}$ , and the lowest  $\mu_{\text{O}}$  value is chosen so that the surfaces have lower energies than the bare closed-ring configuration.

0.28 eV [per  $(1 \times 1)$  surface cell] lower in energy than the open-ring configuration at the same coverage, up from the value of 0.17 eV computed for the bare surfaces. This finding is puzzling in light of the fact that in all  $\beta$ - $\text{Si}_3\text{N}_4$ /rare-earth oxide interfaces imaged in the recent STEM experiments, it is the open-ring termination of the ( $10\bar{1}0$ ) surface that is observed consistently. We, therefore, conclude that the par-

ticular presence of the rare-earth elements or other sintering cations (such as Mg or Al) likely influence the relative stability of the termination of  $\beta$ -Si<sub>3</sub>N<sub>4</sub> matrix grains in their sharp interfaces with rare-earth oxides.

#### IV. SUMMARY

We presented results on and analyses of first-principles calculations for the structural energetics of  $\beta$ -Si<sub>3</sub>N<sub>4</sub> (10 $\bar{1}$ 0) surfaces at  $\Theta = \frac{1}{4}, \frac{1}{2}, \frac{3}{4}$ , and 1 ML oxygen coverages. Our study shows that (i) oxygen has a strong tendency to replace nitrogen in a bridging configuration between two Si atoms rather than attach to the surface epitaxially or interstitially, (ii) oxygenated  $\beta$ -Si<sub>3</sub>N<sub>4</sub> (10 $\bar{1}$ 0) surface exhibits (1 $\times$ 2) reconstructions, and (iii) most lowest-energy surfaces predicted to be stable in the phase diagram are N deficient nonstoichiometric surfaces. These findings, combined with the results from our recent EELS studies at the Si<sub>3</sub>N<sub>4</sub>/CeO<sub>2- $\delta$</sub>  interface,<sup>11</sup> strongly suggest that the Si<sub>3</sub>N<sub>4</sub> open rings are oxygen terminated. We find that the structural stability of most low-energy surfaces is driven by the tendency of surface atoms to saturate their dangling bonds while preserving close-to-ideal coordination (tetrahedral, planar, and bridging) or bond angles. The lowest-energy structure which covers the largest portion of the equilibrium phase diagram is found to be a nonstoichiometric closed-ring configuration at  $\Theta = \frac{3}{4}$  ML oxygen coverage. This closed-ring structure is 0.28 eV lower in energy, per (1 $\times$ 1) cell, than the open-ring structure at the

same coverage. In fact, we find that there is no region of the phase diagram where a surface with an open-ring termination is observed to be the lowest-energy structure. This finding indicates that the relative stability of the open-ring termination over the closed-ring termination, as experimentally inferred from consistent observations of the former in all recent STEM studies, is likely due to the particular presence of the rare-earth element and/or other sintering cations at the interface. Other possibilities for the discrepancy between the experimental and theoretical results so far include (i) the inadequacy of the exchange-correlation functionals used in the present study to capture the subtle energy differences between competing phases (which might necessitate the use of hybrid functionals) or (ii) more complicated surface reconstructions, which could stabilize the open-ring termination, requiring larger supercells than the ones we considered. A deeper understanding of the atomic and electronic structures of the ceramic will naturally require further *ab initio* modeling studies which incorporate oxygen, rare-earth elements, as well as other sintering cations at the interface.

#### ACKNOWLEDGMENTS

This research was supported by the National Science Foundation under Grant No. DMR-0604964 and partially used resources of the National Energy Research Scientific Computing Center, which is supported by the Office of Science of the U.S. Department of Energy.

\*Present address: Department of Physics and Astronomy, Vanderbilt University, Nashville, Tennessee 37235.

<sup>1</sup>*Materials Science and Technology, Structure and Properties of Ceramics*, edited by R. W. Cahn, P. Hassen, and E. J. Kramer (Wiley-VCH, Weinheim, 1994), Vol. 11, pp. 402 and 751.

<sup>2</sup>E. Y. Sun, P. F. Becher, K. P. Plucknett, C. H. Hsueh, K. B. Alexander, S. B. Waters, K. Hirao, and M. E. Brito, *J. Am. Ceram. Soc.* **81**, 2831 (1998); R. L. Satet and M. J. Hoffmann, *J. Eur. Ceram. Soc.* **24**, 3437 (2004).

<sup>3</sup>N. Shibata, S. J. Pennycook, T. R. Gosnell, G. S. Painter, W. A. Shelton, and P. F. Becher, *Nature (London)* **428**, 730 (2004).

<sup>4</sup>A. Ziegler, J. C. Idrobo, M. K. Cinibulk, C. Kisielowski, N. D. Browning, and R. O. Ritchie, *Science* **306**, 1768 (2004).

<sup>5</sup>G. B. Winkelman, C. Dwyer, T. S. Hudson, D. Nguyen-Manh, M. Döblinger, R. L. Satet, M. J. Hoffmann, and D. J. H. Cockayne, *Philos. Mag. Lett.* **84**, 755 (2004); *Appl. Phys. Lett.* **87**, 061911 (2005).

<sup>6</sup>N. Shibata, G. S. Painter, R. L. Satet, M. J. Hoffmann, S. J. Pennycook, and P. F. Becher, *Phys. Rev. B* **72**, 140101(R) (2005).

<sup>7</sup>A. Ziegler, J. C. Idrobo, M. K. Cinibulk, C. Kisielowski, N. D. Browning, and R. O. Ritchie, *Appl. Phys. Lett.* **88**, 041919 (2006).

<sup>8</sup>N. Shibata, G. S. Painter, P. F. Becher, and S. J. Pennycook, *Appl. Phys. Lett.* **89**, 051908 (2006).

<sup>9</sup>A. Ziegler, M. K. Cinibulk, C. Kisielowski, and R. O. Ritchie, *Appl. Phys. Lett.* **91**, 141906 (2007).

<sup>10</sup>K. van Benthem, G. S. Painter, F. W. Averill, S. J. Pennycook,

and P. F. Becher, *Appl. Phys. Lett.* **92**, 163110 (2008).

<sup>11</sup>W. Walkosz, R. F. Klie, S. Ögüt, A. Borisevich, P. F. Becher, S. J. Pennycook, and J. C. Idrobo, *Appl. Phys. Lett.* **93**, 053104 (2008).

<sup>12</sup>L. Benco, *Surf. Sci.* **327**, 274 (1995); P. Dudešek and L. Benco, *J. Am. Ceram. Soc.* **81**, 1248 (1998); T. Nakayasu, T. Yamada, I. Tanaka, and H. Adachi, *ibid.* **81**, 565 (1998); M. Yoshiya, K. Tatsumi, I. Tanaka, and H. Adachi, *ibid.* **85**, 109 (2002); X. Su and S. H. Garofalini, *J. Mater. Res.* **19**, 752 (2004); **19**, 3679 (2004).

<sup>13</sup>G. S. Painter, P. F. Becher, W. A. Shelton, R. L. Satet, and M. J. Hoffmann, *Phys. Rev. B* **70**, 144108 (2004).

<sup>14</sup>P. Rulis, J. Chen, L. Ouyang, W.-Y. Ching, X. Su, and S. H. Garofalini, *Phys. Rev. B* **71**, 235317 (2005).

<sup>15</sup>V. M. Bermudez, *Surf. Sci.* **579**, 11 (2005).

<sup>16</sup>L. Wang, X. Wang, Y. Tan, H. Wang, and C. Zhang, *Chem. Phys.* **331**, 92 (2006).

<sup>17</sup>J. C. Idrobo, H. Iddir, S. Ögüt, A. Ziegler, N. D. Browning, and R. O. Ritchie, *Phys. Rev. B* **72**, 241301(R) (2005).

<sup>18</sup>G. Kresse and J. Hafner, *Phys. Rev. B* **47**, 558 (1993); P. E. Blöchl, *ibid.* **50**, 17953 (1994).

<sup>19</sup>J. P. Perdew and Y. Wang, *Phys. Rev. B* **45**, 13244 (1992); J. Perdew, in *Electronic Structure of Solids '91*, edited by P. Ziesche and H. Eschrig (Akademie, Berlin, 1991), p. 11.

<sup>20</sup>J. P. Perdew, K. Burke, and M. Ernzerhof, *Phys. Rev. Lett.* **77**, 3865 (1996).

<sup>21</sup>G.-X. Qian, R. M. Martin, and D. J. Chadi, *Phys. Rev. B* **38**, 7649 (1988).